Particle trajectories and size sorting above a rippled bed under standing water waves

T. Chu, A. Jarno-Druaux, François Marin, A. Ezersky

Particle trajectories and size sorting above a rippled bed under standing water waves

T. D. Chu,[1,*] A. Jarno-Druaux,[1] F. Marin,[1] and A. B. Ezersky[2]

[1]*Laboratoire Ondes et Milieux Complexes, UMR CNRS 6294 Université du Havre, 25 rue Philippe Lebon, B.P. 540, F-76058 Le Havre Cedex, France*

[2]*Laboratoire Morphodynamique Continentale et Côtière, UMR CNRS 6143 Université de Caen, 2-4 rue des Tilleuls, F-14000 Caen, France*

(Received 7 June 2011; revised manuscript received 9 December 2011; published xxxxx)

Particle trajectories and size sorting above an artificial rippled bed under standing surface waves are experimentally and theoretically studied. It is observed that fine particles may be trapped in a very thin region near the ripple crests. When the surface waves damp, fine particles concentrate on the top of ripple crests forming narrow strips, while coarse particles settle more uniformly along the rippled bed. Measurements of particle concentrations before their deposition confirm this size segregation. The present experimental results are explained with a theoretical approach.

DOI: 10.1103/PhysRevE.00.001300 PACS number(s): 45.70.Mg, 45.70.Qj

I. INTRODUCTION

Periodic patterns with typical wavelengths of ≈10 cm often cover seabeds in coastal zones. These structures, generally called ripples, result from complex interactions between the flow of water and the granular bottom. Since the pioneering works of Ayrton [1] and Bagnold [2], the formation of vortex ripples induced by oscillatory motion has been intensively studied. Many experimental and theoretical works have been conducted on the morphology of these structures, which significantly affect sediment transport, wave damping, and boundary layer structure. The wavelength of ripples is roughly proportional to the amplitude of the water motion [3], and the flow in their vicinity is dominated by the generation and ejection of lee-side coherent vortices [4–6]. Detailed visualizations of vortex dynamics have been carried out [7–9].

A majority of the literature devoted to ripple patterns considers the case of homogeneously sized grains [10–12]; however, sediments in coastal zones are usually heterogeneous in size. It should be noted that pattern formation in granular materials containing different particles is widely investigated now [13]. However, the studies of grain segregation for ripples under waves are scarce. A surface sorting is reported: coarse sediments are observed to accumulate mostly along the ripple crests, while fine grains mostly accumulate in the troughs [14–16]. The presence of fine particles forming very narrow strips on the top of crests is mentioned in [16]. In the case of standing waves, sand bar formation is observed with bar crests composed of coarse sand and flat plateaus of fine sand [17]. The density segregation under decaying highly nonlinear waves, solitons, is considered in Ref. [18]. Light grains concentrate in a narrow region close to the ripple crests when the waves are damped. The sorting process was not analyzed in detail in Ref. [18]. The aim of the present work is to study the segregation process above a rippled bed under a simple oscillating flow, standing waves, from a detailed analysis of the motion of individual particles of different sizes. Grain trajectories under standing waves and decaying standing waves are experimentally obtained, and concentrations of sinking particles are measured before their deposition on the bed. There is only a restricted number of experimental studies on granular material dynamics dealing with trajectories of individual particles [19]. Present measurements improve the theoretical model for the flow above ripple crests proposed in Ref. [18]. Finally, a model for the flow above ripple troughs is suggested to complete the explanation of the experimental results.

This paper is organized as follows. In Sec. II, a short description of the experimental setup is given. The experimental results are presented in Sec. III. Sec. IV is devoted to the $f_r = 0.31$ theoretical approach. The theoretical results are compared with the experimental findings. The paper ends with conclusions in Sec. V.

II. EXPERIMENTAL SETUP AND PROCEDURE

The experiments were conducted in a 5.4-m-long, 0.3-m-wide wave flume. Surface waves are generated by an oscillating paddle at one end of the flume; a near-perfect reflection takes place at the other end. The frequency of the oscillating paddle is chosen close to the resonant frequency Hz of the mode whose wavelength is equal to the effective flume length ($L_w = 5$ m). The water depth at rest h is 0.26 m. The height and the period of the wave are measured with two resistive probes. For the present tests, the maximum wave height at the antinode H is 0.04 m. Ripples were generated beneath standing waves from an initially flat bed, which consisted in a 4-cm layer of polyvinyl chloride (PVC) grains of density $\rho_p = 1350$ kg.m^{-3} and median diameter $d_p =$ 0.20 mm. Ripples formed rapidly along the flume once the wave maker was switched on. Their size and shape change from one end of the flume to the other end, depending on their position in relation to the position of the nodes and antinodes of the standing wave. The regions under the antinodes are essentially flat, whereas the regions under the nodes where the bed shear stress is maximum are covered by the greatest ripples. When the equilibrium state is reached, we switch off the oscillating paddle and empty slowly the wave flume in order to maintain the natural form of the bed. The rippled bed is then covered by a thin powdering of cement. When this powdering is dry, the wave flume is refilled with the same water level at rest as previously (0.26 m). PVC particles are then carefully injected through the free surface above

*tien-dat.chu@univ-lehavre.fr.

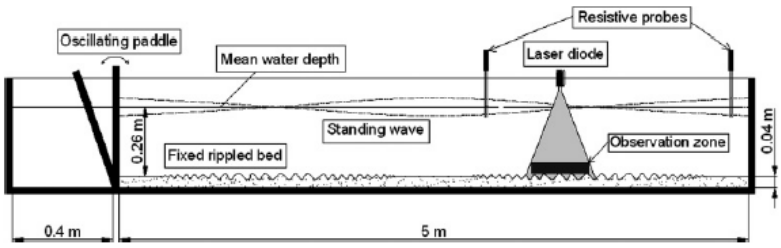

FIG. 1. Side view of the flume.

the fixed rippled bed, and their trajectories are registered. The flow conditions change along the wave flume and the Reynolds number, $\mathrm{Re} = U_\infty a/\nu$, varies in the range $0 < \mathrm{Re} < 5700$, where $U_\infty = a\omega = \pi H/[T \times \sinh(kh)]$ is the velocity of fluid particles at the edge of the bed boundary layer, a is the orbital amplitude of fluid particles at the same place, ω is the wave pulsation, T is the wave period, ν is the water kinematic viscosity, and k is the wave number. The edge of the bottom boundary layer may be estimated at the height k_s above the level midway between crest and trough of the ripples [20], where k_s is the Nikuradse roughness length, which may be estimated for a ripple bed by $k_s = 25H_r^2/L_r$ [21]. The studied zone for the particle trajectories and the sediment sorting is chosen close to the node located in the vicinity of the wall reflecting the surface waves (Fig. 1). In this zone, ripples are mostly regular and bidimensional; their wavelength L_r and their height H_r are, respectively, 5.5 and 1.5 cm, and we have $\mathrm{Re} \approx 4500$. The mobility number (Ψ), the Stokes sedimentation velocity (U_0), and the Stokes number (St) are calculated as follows: $\Psi = (a\omega)^2/d_p g(s-1)$, $U_0 = d_p^2(\rho_p - \rho_w)g/18\nu\rho_w$, and $\mathrm{St} = d_p^2\rho_p\omega/18\nu\rho_w$, where g is the acceleration due to gravity, s is the relative density of grain, and ρ_w is the fluid density. The Shields number θ may be estimated with $\theta = 0.5 f_w \Psi$, where f_w is the friction factor. Following Davies [22], the flow regime depends on the values of Re and a/k_s ; this regime is rough turbulent in the considered zone. Five different kinds of PVC particles have been used, as specified in Table I showing the experimental conditions; the hydrodynamic forcing is the same for all of the tests. Tests 1 to 5 were carried out with well size-sorted particles (P_1 to P_5), while Test 6 involved a mixture of 50 % (in weight) very fine particles (P_1) and 50 % medium particles (P_3) and Test 7 involved a mixture of 50 % very fine particles (P_1) and 50 % coarse particles (P_5).

Grain trajectories were obtained performing particle tracking velocimetry (PTV). The principle of PTV is to individually follow each introduced particle in successive images. A high-resolution camera Dalsa Falcon PT-41-4M60 (resolution 2352 × 1728 pixels), 62 frames per second, is used in combination with a laser diode, which generates a thick vertical light sheet. The thickness of the light sheet is fixed to two centimeters so that particles stay long enough in the illuminated area to enable the capture of grain trajectories over several wave periods [23,24]. Particle trajectories are obtained using a program presented in Ref. [25] and adapted to the present experiments. For present tests, two phases of the flow were considered: during the excitation of standing waves [phase (1)] and during the decay of surface waves [phase (2)], after the stopping of the oscillating paddle. The dimensions of the observation window of the video camera are fixed to one ripple wavelength in the vertical direction, one ripple wavelength in the horizontal direction for the phase 1 and four ripple wavelengths for the phase 2. The large horizontal area for phase 2 allows accurate study of the sediment sorting and the settling zones for decaying waves, when the horizontal zoom in on one ripple length for phase 1 provides very precise information on particle trajectories close to the ripple crests, as shown in the next section.

III. EXPERIMENTAL RESULTS

A. Particle motion in the vicinity of ripple crests during the excitation of standing waves

Organized vortices are formed on the lee side of ripples and shed above ripple crests each half-cycle [20,26]. Figure 2(a) depicts a typical trajectory above the rippled bed under the effect of vortices showing the complex motion of particles. Let us focus on the area close to ripple crests. The oscillating movement of particles in a zone confined just above the top of the ripple crests can be observed, as shown in Fig. 2(b). In this confinement zone, particles can be "captured" [Figs. 2(b) and 2(c)] and ejected in the flow several periods later [Fig. 2(d)]. Form and dimensions of the confined zone are determined by the extreme positions of grains that oscillate in it. Its lower limit is the ripple crest and its height varies from zero at its

TABLE I. Experimental conditions.

Particle	s	d_p (mm)	U_0 (mm/s)	U_∞/U_0	St	Ψ
P_1	1.35	0.11	2.1	51.4	1.6×10^{-3}	29.9
P_2	1.35	0.19	5.8	18.5	4.5×10^{-3}	17.9
P_3	1.35	0.28	13.2	8.2	10.2×10^{-3}	11.9
P_4	1.35	0.45	33.4	3.2	25.8×10^{-3}	7.5
P_5	1.12	0.57	18.1	5.9	33.7×10^{-3}	17.3

Test number	Particle
1	P_1
2	P_2
3	P_3
4	P_4
5	P_5
6	50 % P_1 –50 % P_3
7	50 % P_1 –50 % P_5

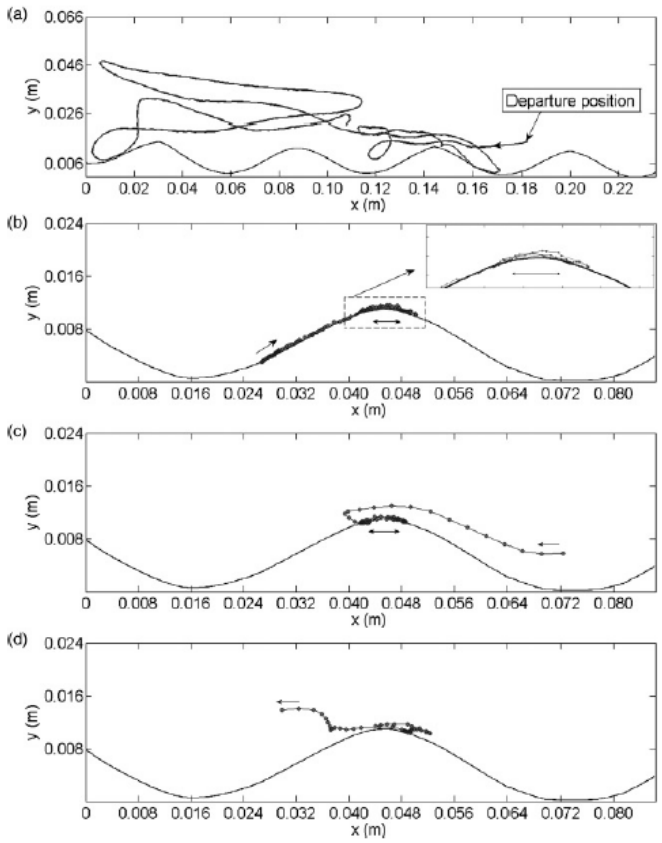

FIG. 2. Typical particle trajectories. (a) Particle trajectory under the action of vortices, Test 1; (b) Rolling of a particle along ripple side and "capture" in the confinement zone, Test 2; (c) "Capture" of a suspended particle, Test 2; (d) "Ejection" of a particle from the confinement zone, Test 4.

extremities to $H_{cz} = 0.9$ mm at the top of the ripple crest; this height is comparable with the Stokes layer thickness, $\delta = \sqrt{2\nu/\omega} \approx 1$ mm, and is greater than the grain size. The length L_{cz} of the confinement zone may be estimated at 10.9 mm, which corresponds approximately to one-fifth of the ripple wavelength in the tested zone. Present tests show that the ejected particles are the ones for which the diameter d_p is greater than approximately 0.28 mm. These particles are more exposed to the vortices than finer ones. We measured the mean resident time of particles in the confinement zone according to the sediment size. This time varies from one-half to two or three times the wave period for coarse particles. It is much longer for very fine and fine particles, ranging from three times the wave period to the total duration of the experiment. The grains capture and ejection at ripple crests may be considered as a sediment sorting process. The existence of a confinement zone is taken into account in the theoretical approach which is presented in Sec. IV.

B. Particle trajectories during the decay of surface waves

When the oscillating paddle is stopped, suspended particles start to settle under the action of gravity. Let us consider that the time $t = 0$ is the instant corresponding to the stopping of the oscillating paddle. The settling velocity of the coarse particles ($d_p = 0.45$ mm, Test 4) is about 15 times larger than the one for the very fine particles ($d_p = 0.11$ mm, Test 1). As shown in Fig. 3(a), the amplitude of motion of coarse particles before they reach the bed is large, since these particles begin to settle rapidly after a few wave periods ($t \approx 2$–$3\ T$) when the hydrodynamic forcing is still intense. Coarse particles generally reach the bed after a trajectory composed of four lateral excursions in the observation window. On the other hand, finer particles, which are lighter [Figs. 3(b)–3(d)], reach the bed later when the amplitude of fluid motion is weaker; the number of lateral excursions increases when particle size decreases. The maximum number of lateral excursions is equal to 10 for very fine particles ($d_p = 0.11$ mm). The ratio of the amplitude of the lateral extension of particle excursion a_p on the amplitude of the fluid motion a outside the boundary layer in the dynamical phase [phase (1)] used as a reference fluid amplitude is estimated. Typical values of a_p/a are 0.45 and 0.1 for coarse (Test 4) and very fine particles (Test 1), respectively, when they arrive in the observation window. These values decrease as particles approach the bed. About 100 trajectories of sinking particles have been measured. Initial positions of these particles at the upper limit of the observation window are

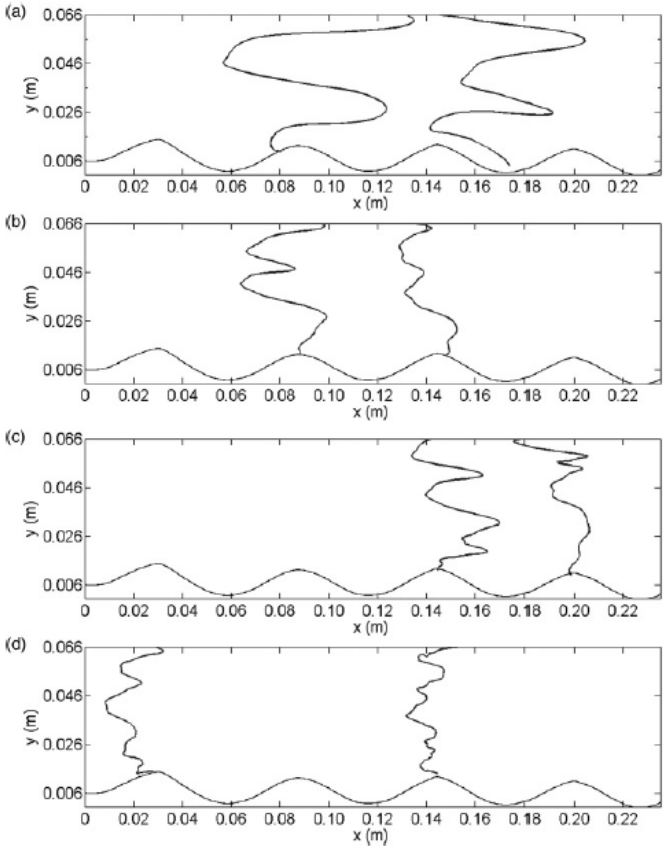

FIG. 3. Typical particle trajectories during the waves damping. (a) Test 4; (b) Test 3; (c) Test 2; (d) Test 1.

uniformly distributed above ripples. Places where the grains settle along the rippled bed are analyzed according to their size. The histogram of repartition of particles deposition zone over the three regions delimiting the crest, trough, and both sides is shown in Fig. 4. The length of the region defining the vicinity of ripple crest is fixed to 10 mm (18 % of the ripple wavelength in the considered zone) divided equally on both sides of the top of the ripple. The length of the trough region is estimated at 16 mm; both sides occupy 29 mm. The results show that 61 % of the very fine and medium particles (Tests 1 to 3) settle in the vicinity of the ripple crests, whereas 39 % of these particles settle elsewhere. In the case of coarse particles (Tests 4 and 5), only 29 % of grains settle in the vicinity of the crests. Furthermore, for the range of coarse particles considered herein, no privileged deposition place is noted. Let us consider the temporal evolution of particle concentrations just above the rippled bed when the surface waves damp.

C. Suspension sorting during the decay of surface waves

Figure 5 depicts the area in which particle concentrations have been obtained; this area is a 1-cm-high horizontal strip. Its lowest level is 2.9 mm above the highest point of the bed. Zones delimiting regions above ripple crests (10 mm long) and above ripple troughs (16 mm long) are defined in the legend of Fig. 5. Particle concentrations per unit area have been obtained in the following way: the number of particles crossing the strip is counted during their settling when the water waves damp.

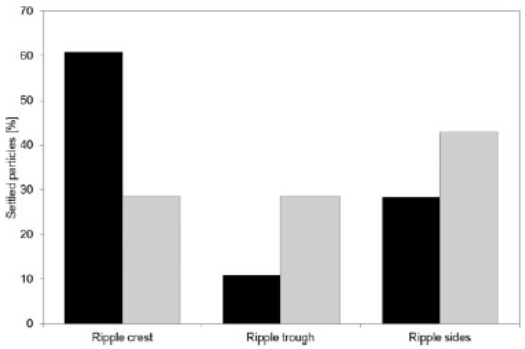

FIG. 4. Distribution of settled particles along the rippled bed surface. Black column: medium, fine, and very fine particles (Tests 1, 2, and 3, respectively); gray column: coarse particles (Tests 4 and 5).

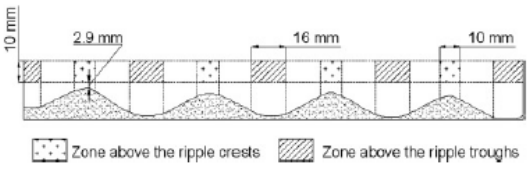

FIG. 5. Area above the rippled bed where particle concentrations have been measured.

The strip is in a vertical plane illuminated by a laser diode (Fig. 1). The particles concentration C is estimated along the strip as $C = n/S$, where n is the number of detected particles in the considered zone and S is the surface of this zone.

The temporal evolution of relative concentration $C/C_{\max}$ is shown in Fig. 6, where $C_{\max}$ is the maximum concentration measured over all the experiments during the settling process. The relative error of concentration measurement is related to the particle detection process in the horizontal strip performed in the Matlab program. It is estimated at 5 % and depicted in Fig. 6 with error bars. The origin of temporal axis $t = 0$ corresponds to the time where the oscillating paddle is stopped. This figure exhibits an exponential decrease of $C/C_{\max}$ with t/T. Using a best-fit procedure, the temporal variation of particle concentration may be estimated with the following equations:

$$C/C_{\max} = 1.49e^{(-0.268t/T)}, \quad 0.45 \leqslant d_p \leqslant 0.57 \text{ mm, ripple crest and trough,} \tag{1}$$

$$C/C_{\max} = 1.16e^{(-0.032t/T)}, \quad 0.11 \leqslant d_p \leqslant 0.28 \text{ mm, ripple crest,} \tag{2}$$

$$C/C_{\max} = 1.11e^{(-0.039t/T)}, \quad 0.11 \leqslant d_p \leqslant 0.28 \text{ mm, ripple trough.} \tag{3}$$

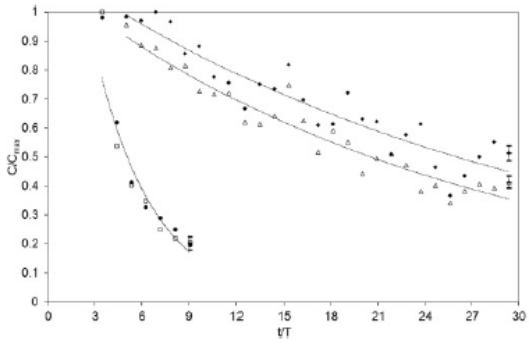

FIG. 6. Temporal evolution of particle concentrations close to the bed when the surface waves damp. ♦ Above ripple crest: $0.11 \leqslant d_p \leqslant 0.28$ mm (Tests 1, 2, and 3). Δ Above ripple trough: $0.11 \leqslant d_p \leqslant 0.28$ mm (Tests 1, 2,and 3). • Above ripple crest: $0.45 \leqslant d_p \leqslant 0.57$ mm (Tests 4 and 5). □ Above ripple trough: $0.45 \leqslant d_p \leqslant 0.57$ mm (Tests 4 and 5). The curves represent the trendlines obtained using a best-fit procedure.

The particles in the size range $0.45 \leqslant d_p \leqslant 0.57$ mm settle rapidly and regularly without significant difference between the concentrations above the ripple crests and troughs. As far as the particles in the size range $0.11 \leqslant d_p \leqslant 0.28$ mm are concerned, the two plotted curves exhibit similar variations and a trend to higher concentration above the crests that can be interpreted as a size sorting above the rippled bed during the particle settling when the surface waves damp. The concentration distributions show temporal fluctuations in the size range $0.11 \leqslant d_p \leqslant 0.28$ mm when these distributions are more regular for coarser grains. These are the result of the high sensitivity of the light particles to the fluid movement until the water becomes totally still.

D. Particle sorting after the decay of surface waves

In this section, we consider the final state for Tests 6 and 7, when the water waves are damped. Figure 7(a) shows the grain sorting at the end of Test 6 involving a mixture with 50 % of very fine particles ($d_p = 0.11$ mm) and 50 % of medium particles ($d_p = 0.28$ mm). Based on the observation of Fig. 7(a), one ripple wavelength is split in five regions defined on this figure: (i) designates the region on the top of the crest; (ii) is the region nearby (i) directed toward the fixed end of the wave flume; (iii), (iv), and (v) are, respectively, the ripple side toward the fixed end of the flume (right ripple side), the ripple trough, and the ripple side toward the oscillating paddle (left ripple side). A calculation to estimate the proportions of covering for each type of grain has been carried out. This process consists in affecting ranges of color levels to very fine and medium particles and in counting the number of pixels associated to the two categories of grains in each region. The pixels uncovered by particles are also counted. The results are reported in Fig. 7(b) as percentages. Average values are calculated in each zone. The top of the crest (i) is almost saturated in very fine particles covering 82 % of this region, while the nearby region (ii) is covered essentially by medium grains (70 %). For the three other regions, very fine and medium particles are present composing a mixture. For standing waves above a flat bed, the steady drift takes the form of closed recirculating cells with boundaries at a spacing of one-quarter the wavelength of the surface waves [27,28]. Very close to the bed that is inside the Stokes boundary layer thickness, the fluid particle drift is oriented toward the node of the water surface profile and away from the antinodes. However, the drift is in the opposite direction further in the outer flow. Present tests are carried out above a rippled bed, and vortices are generated leading to suspended load transport. As shown in Fig. 1 (Sec. II), the particle trajectories are recorded between the antinode of the surface wave in the central part of the flume and the node close to the fixed end of the channel, where the drift is oriented toward the wave paddle, outside the Stokes layer. A possible reason for the settling of medium particles on the right ripple sides forming strips close to the ripple crests is the effect of drift velocity leading to vortices formed more vigorously during one half-cycle than during the other. The vortices generated above the left ripples sides are stronger than the ones formed above the right sides; at flow reversal, these vortices move toward the right sides carrying particles. The medium particles settle on the bottom when the vortices intensity is still high. The very

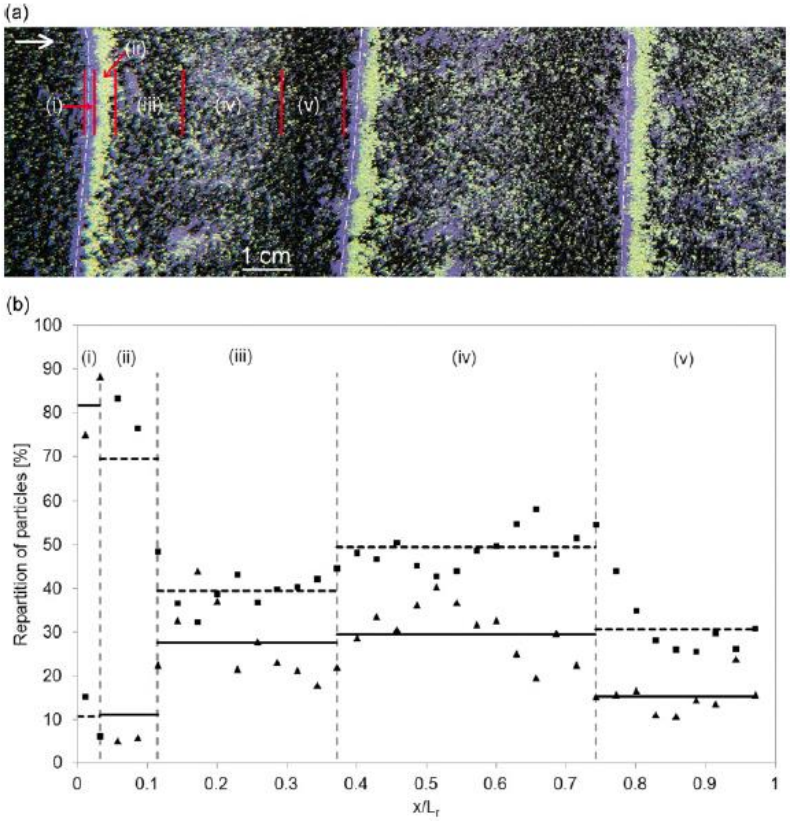

FIG. 7. (Color online) (a) Sediment sorting on the bed at the end of Test 6. The dashed lines represent the ripple crests positions. The arrow depicts the direction from the wave paddle to the fixed vertical end of the flume. Ripple crests are covered by very fine particles [violet (gray) grains]; a strip of medium particles [light beige (white) grains] is located nearby each crest. Very fine and medium particles are observed on the ripple troughs and sides. (i)–(v) Designate the five regions along one ripple wavelength used to evaluate the particle covering. (b) Repartition of particles over one ripple wavelength at the end of Test 6. Limits between different regions (vertical dashed lines); averaged values of medium particles distribution (horizontal dashed lines); averaged values of fine particles distribution (horizontal solid lines). (▲) Very fine particles; (■) medium particles.

fine particles fall later, when the vortices intensity is weaker and the asymmetry becomes negligible.

For Test 7, which was carried out with a mixture with 50 % of very fine particles ($d_p = 0.11$ mm) and 50 % of coarse particles ($d_p = 0.57$ mm), approximately the same particle segregation was qualitatively observed as for Test 6, the coarse particles taking the role of the medium particles used for Test 6. We can just note that the relative narrow strips of medium particles, which were observed in region (ii) for Test 6, were wider for the coarse particles of Test 7. These observations are explained in the next section with a theoretical approach.

IV. THEORETICAL APPROACH

We present in this section an improvement of the theoretical model proposed in Ref. [18] for the flow above ripple crests and a simple model for the flow above ripple troughs, to explain the present experimental results on the sorting of particles under damping waves. The model presented in Ref. [18] was not based on a detailed analysis of particle trajectories above a rippled bed; the process of grain segregation was not considered in detail. Present experimental results for particle trajectories show us in particular that close to ripple crests, particles oscillate. The model previously developed in Ref. [18], which had as specificity a fixed hyperbolic point at ripple crest, had to be improved to take into account the oscillating movement of particles in a small zone just above the ripple crest (confinement zone). This consideration affects the particle trajectories and the settling zones.

A. Improvement of the theoretical model proposed in Ref. [18] for the flow above ripple crests

A very simple model in a narrow region near ripple crests was considered in Ref. [18], taking into account only the Stokes

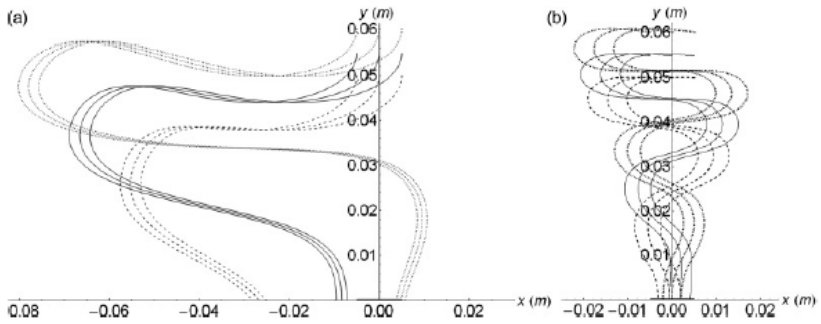

FIG. 8. Theoretical trajectories starting from nine different initial points above the ripple crest. (a) $d_p = 0.45$ mm; (b) $d_p = 0.28$ mm. The solid bold line on the x axis depicts the area near the ripple crest.

force, and assuming in the first approximation that the bottom is flat. The flow was modeled in the vicinity of each crest by the stream function, $\psi = -a(\alpha x + y)y$, where x and y are the horizontal and vertical coordinates. The point $x = 0$, $y = 0$ corresponds to ripple crests. The coefficient $\alpha = \alpha_0 \sin(\omega t)$ is the parameter that controls the slope of the line separating the forward and return flows. The value of α_0 may be estimated from present tests from flow visualization: $\alpha_0 \approx 1$ rad. The coefficient $a = a_0 \sin(\omega t)$ is related to the vorticity $\vec{\Omega} = 2a\vec{z}$, where $\vec{z}$ is a unit vector perpendicular to the flow plane. A slip condition is assumed on the bed surface $y = 0$, and the influence of viscosity was neglected outside the Stokes layer. It was supposed that this thickness is much less than the other characteristic scales of motion in the vicinity of the ripple crest. A particularity of the flow was the presence of a hyperbolic point with a stationary position at $x = 0, y = 0$. Present experimental results show (Sec. III A) that close to ripple crests, particles oscillate in a confinement zone. An improvement of the model presented in Ref. [18] consists in introducing an oscillating movement of the hyperbolic point. We suggest modeling the flow in the vicinity of ripple crests by the following stream function: $\psi = -a[\alpha(x + x_0)y + y^2]$, where $x_0 = X_0 \sin(\omega t)$. X_0 is the amplitude of the movement of hyperbolic point and is considered to correspond to half of the length of the confinement zone. The horizontal (U_x) and vertical (U_y) components of the flow velocity vector are obtained from the stream function:

$$U_x = \frac{\partial \psi}{\partial y} = -a[\alpha(x + x_0) + 2y], \tag{4}$$

$$U_y = -\frac{\partial \psi}{\partial x} = a\alpha y. \tag{5}$$

The particle velocity $\vec{V}$ does not coincide with the flow velocity $\vec{U}$. For our experimental conditions, the Stokes number is a small parameter ($St \sim 10^{-3}, 10^{-2}$) that we use as an expansion parameter. The particle velocity is written as

$$\vec{V} = \vec{V}^{(0)} + \mathrm{St}\vec{V}^{(1)} + \mathrm{St}^2\vec{V}^{(2)} + \cdots \tag{6}$$

Neglecting all terms proportional to St^2 in Eq. (6), the particle velocity field may be written as follows [18]:

$$V_x = U_x - \frac{\mathrm{St}}{\omega}\sigma\frac{dU_x}{dt}, \tag{7}$$

$$V_y = U_y - U_0 - \frac{\mathrm{St}}{\omega}\sigma\frac{dU_y}{dt}, \tag{8}$$

where V_x and V_y are the projections of the particle velocity vector onto the horizontal and vertical directions, and $\sigma = 1 - \rho_w/\rho_p$. After the substitution of Eqs. (4) and (5) into Eqs. (7) and (8), we obtain the following expressions for the particle velocities close to the ripple crests:

$$V_x = -a[\alpha(x + x_0) + 2y] + \frac{\mathrm{St}}{\omega}\sigma[(\dot{a}\alpha + a\dot{\alpha})(x + x_0) + 2\dot{a}y - a^2\alpha^2(x + x_0) + a\alpha\dot{x}_0], \tag{9}$$

$$V_y = a\alpha y - U_0 - \frac{\mathrm{St}}{\omega}\sigma[(\dot{a}\alpha + a\dot{\alpha})y + a^2\alpha^2 y]. \tag{10}$$

It is supposed that after the oscillating paddle is stopped, the turbulence decays much more rapidly than the waves. During the wave damping, it is reasonable to consider that the vorticity and the length of the confinement zone decay in the same way as the amplitude of the surface waves. We suppose that the change of the amplitude of particles velocity during a wave period is small compared with the particles velocity amplitude. The particles velocity temporally averaged over a wave period $T = 2\pi/\omega$ is easily obtained from Eqs. (9) and (10):

$$\langle V_x \rangle = -a_0\alpha_0 e^{-2\gamma t}\left[\frac{1}{2} + \frac{\mathrm{St}}{\omega}\sigma\left(\gamma + \frac{3}{8}a_0\alpha_0 e^{-2\gamma t}\right)\right]x, \tag{11}$$

$$\langle V_y \rangle = a_0\alpha_0 e^{-2\gamma t}\left[\frac{1}{2} + \frac{\mathrm{St}}{\omega}\sigma\left(\gamma - \frac{3}{8}a_0\alpha_0 e^{-2\gamma t}\right)\right]y - U_0, \tag{12}$$

where γ is the rate of exponential decay of surface waves.

The horizontal component $\langle V_x \rangle$ is negative for $x > 0$ and positive for $x < 0$, and particles tend to move toward the ripple crest ($x = 0$) when the surface waves damp. The rate of exponential decay for the present surface waves is estimated at $\gamma = 0.021\ \mathrm{s}^{-1}$ from measurements of the temporal evolution of surface waves using resistive probes. Figure 8 shows typical particle trajectories for different initial positions and two median diameters: $d_p = 0.45$ mm and $d_p = 0.28$ mm. The vertical coordinates of these initial positions are chosen close to the upper bound of the observation window considered in Secs. II and III (one ripple length high). The fine particles

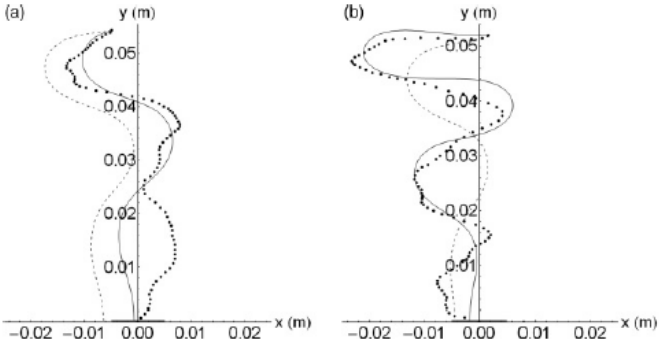

FIG. 9. Comparison of theoretical and experimental particle trajectories. (a) $d_p = 0.28$ mm; (b) $d_p = 0.19$ mm. Present measurements (dotted line); Ezersky and Marin's (2008) model (dashed line); present model (solid line). The solid bold line on the x axis depicts the area near the ripple crest.

($0.11 \leqslant d_p \leqslant 0.28$ mm) are found to settle close to ripple crests when the coarser ones may fall everywhere on the bed. These particles settle on the bottom after only a few wave periods; Fig. 6 exhibits that most of them reach the area very close to the bottom approximately for $4 \leqslant t/T \leqslant 9$, when the damping time of surface waves is much greater ($1/\gamma \approx 48$ s $\approx 15\ T$). For $d_p \leqslant 0.28$ mm, the time for particles to reach the bottom is greater; Fig. 6 shows that when $t/T = 30$, particles are not all deposited on the bed. The settling area near the ripple crests is well predicted by the present theoretical model. Experimental and theoretical particle trajectories are depicted in Fig. 9; this figure shows that the present adjustment of the model proposed in Ref. [18] significantly improves the prediction of particle trajectories and deposition areas.

B. Model of flow above ripple troughs

The vorticity field above an artificial rippled bed under waves was considered in Ref. [20]. It was shown that the values of the vorticity are much weaker above ripple troughs than close to ripple crests (except very close to the bed). A sketch of the rippled bed is depicted in Fig. 10. It can be seen that the "angles of ripple troughs" slightly vary along the bed; the averaged value is 135°.

Let us consider the classical model of potential flow for a 135° angle:

$$f(z) = \beta(ze^{-i\pi/8})^{4/3}, \tag{13}$$

where z is a complex variable, $z = x_1 + iy_1$, $i^2 = -1$, and $\beta = \beta_a \cos(\omega t)$ for an oscillating flow; the point $x_1 = 0$, $y_1 = 0$ corresponds to ripple troughs. Using this model, which takes into consideration the curvature of the streamlines in the ripple troughs, we are able to understand qualitatively why particles settle in the ripple troughs. The complex function of the flow may be written in the following way:

$$f(z) = \varphi + i\psi = \beta\left(re^{i\theta}e^{-\frac{i\pi}{8}}\right)^{\frac{4}{3}} = \beta r^{\frac{4}{3}}\left(\cos\frac{4}{3}\left(\theta - \frac{\pi}{8}\right) + i\sin\frac{4}{3}\left(\theta - \frac{\pi}{8}\right)\right), \tag{14}$$

where φ and Ψ are the potential and stream functions, respectively, $r = \sqrt{x_1^2 + y_1^2}$, and θ is the polar angle. Using the Cartesian coordinates U_{x_1} and U_{y_1} for the flow velocity components, we get

$$U_{x_1} = U_r\cos\theta - U_\theta\sin\theta = \frac{4}{3}\beta r^{1/3}\cos\left(\frac{\theta}{3} - \frac{\pi}{6}\right), \tag{15}$$

$$U_{y_1} = U_r\sin\theta + U_\theta\cos\theta = -\frac{4}{3}\beta r^{1/3}\sin\left(\frac{\theta}{3} - \frac{\pi}{6}\right), \tag{16}$$

where U_r and U_θ are the radial and orthoradial coordinates of the flow velocity vector, respectively.

Substituting Eqs. (15) and (16) into Eqs. (7) and (8), we get the instantaneous particle velocities after some transformations:

$$V_{x_1} = \frac{4}{3}\beta\left(x_1^2 + y_1^2\right)^{1/6}\cos\left[\frac{\arctan(y_1/x_1)}{3} - \frac{\pi}{6}\right] - \frac{\mathrm{St}}{\omega}\sigma\left\{\frac{4}{3}\dot{\beta}\left(x_1^2 + y_1^2\right)^{1/6}\cos\left[\frac{\arctan(y_1/x_1)}{3} - \frac{\pi}{6}\right] + \frac{16}{27}\beta^2\left(x_1^2 + y_1^2\right)^{-2/3}x_1\right\}, \tag{17}$$

$$V_{y_1} = -\frac{4}{3}\beta\left(x_1^2 + y_1^2\right)^{1/6}\sin\left[\frac{\arctan(y_1/x_1)}{3} - \frac{\pi}{6}\right] - U_0 - \frac{\mathrm{St}}{\omega}\sigma\left\{-\frac{4}{3}\dot{\beta}\left(x_1^2 + y_1^2\right)^{1/6}\sin\left[\frac{\arctan(y_1/x_1)}{3} - \frac{\pi}{6}\right] + \frac{16}{27}\beta^2\left(x_1^2 + y_1^2\right)^{-2/3}y_1\right\}. \tag{18}$$

Figure 11 shows typical comparisons between theoretical and experimental trajectories above ripple trough. The initial vertical coordinate of theoretical trajectories is chosen close to the ripple height H_r. The parameters of flow and particle are the ones that were used in the model above the ripple crest; β is estimated using the model of flow velocity at the upper edge of the bottom boundary layer. Although the

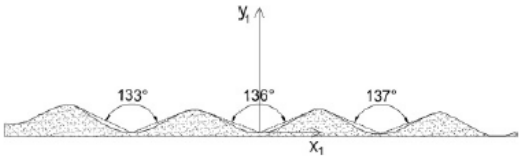

FIG. 10. Sketch of the rippled bed.

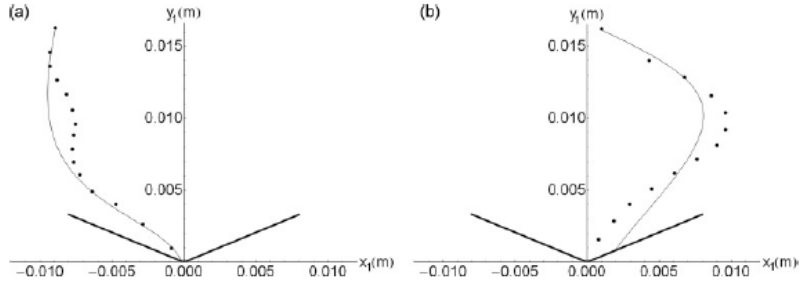

FIG. 11. Comparison between theoretical [Eqs. (17) and (18)] and experimental particle trajectories. Bold lines forming an angle represent the ripple trough region; present model (solid lines); present measurements (dotted lines). (a) $d_p = 0.45$ mm; (b) $d_p = 0.28$ mm.

theoretical trajectories are simpler than the experimental ones, a qualitative agreement is obtained.

Assuming an exponential decay of the flow, $\beta = \beta_a \cos(\omega t)e^{-\gamma t}$, it is easy to obtain the particles velocity field temporally averaged over one wave period:

$$\langle V_{x_1} \rangle = -\frac{8}{27}\frac{\mathrm{St}}{\omega}\sigma\beta_a^2 e^{-2\gamma t}\left(x_1^2 + y_1^2\right)^{-2/3} x_1, \qquad (19)$$

$$\langle V_{y_1} \rangle = -U_0 - \frac{8}{27}\frac{\mathrm{St}}{\omega}\sigma\beta_a^2 e^{-2\gamma t}\left(x_1^2 + y_1^2\right)^{-2/3} y_1. \qquad (20)$$

It should be noted that our model cannot be applied for coordinates corresponding to positions very close to the bed, because the influence of viscosity must be taken into consideration for these positions. The averaged vertical velocity of particles induced by the oscillating flow is directed toward the ripple trough, due to centrifugal forces acting on particles moving in a flow near a concave wall. The averaged horizontal velocity of particles is negative for $x_1 > 0$ and positive for $x_1 < 0$, and particles tend to converge toward the ripple trough according to Eqs. (19) and (20). Using Eqs. (11), (12), (19), and (20), it can be emphasized that the ratio between the vertical and horizontal components of particle velocities is much smaller near the ripple crest than in the ripple trough. It means that a particle in the vicinity of a ripple crest will converge more strongly toward this crest than a particle with the same diameter above a ripple trough will converge toward the trough. Comparing Eq. (12) with Eq. (20) for the averaged vertical velocity of particles, it is possible to conclude that the particles settling time is greater near the ripple crest than near the ripple trough. The centrifugal effect near the concave wall leads to an averaged velocity in the same direction as the gravity force. In other words, coarse particles settle rapidly on the bed before the damping of surface waves, and fine particles with smaller settling velocities are more affected by the mean horizontal velocities toward the ripple crest than coarser particles. Then, an accumulation of fine particles appears at ripple crests when the surface waves are completely damped, as observed in the present experiments (Sec. III).

V. CONCLUSIONS

This paper presents an experimental and theoretical study of particle size sorting above an artificial rippled bed under standing water waves. Present tests were carried out in a 5.4-m-long wave flume with lightweight grains; two phases were considered: during the excitation of standing waves [phase (1)] and during the decay of surface waves [phase (2)]. Particle trajectories were obtained for the two phases with a high-resolution camera. In the first phase, fine and medium particles ($0.11 \leqslant d_p \leqslant 0.28$ mm) are trapped in a thin confinement zone, approximately one Stokes boundary layer thickness high, close to ripple crests. In the second phase, trajectories and deposition zones of particles on the rippled bed strongly depend on their size. Most of fine and medium particles fall in the vicinity of ripple crests when coarser particles ($0.45 \leqslant d_p \leqslant 0.57$ mm) settle more uniformly along the rippled bed, with nevertheless an asymmetry in the deposition zones due to the mean flow induced by standing waves near the bottom. Measurements of particles concentration close to the bottom show a size segregation during the wave damping, when particles are still in suspension: the concentrations of the finest tested particles is higher above the ripple crest than above ripple trough, when no significant difference can be noted for coarser particles. An improvement of the model proposed in Ref. [18] for the flow above ripple crests and a simple model for the flow above ripple troughs explain the present experimental results. Further research is needed to consider particle size segregation with active beds.

ACKNOWLEDGMENT

Financial support by the Haute-Normandie region ("Scale" Network) is gratefully acknowledged.

[1] H. Ayrton, Proc. R. Soc. London, Ser. A **84**, 285 (1910).
[2] R. A. Bagnold, Proc. R. Soc. London, Ser. A **187**, 1 (1946).
[3] T. Schnipper, K. Mertens, C. Ellegaard, and T. Bohr, Phys. Rev. E **78**, 047301 (2008).
[4] K. H. Andersen, M. L. Chabanol, and M. V. Hecke, Phys. Rev. E **63**, 066308 (2001).
[5] A. G. Davies and P. D. Thorne, J. Geophys. Res. **110**, C05017 (2005).

[6] V. Marieu, P. Bonneton, D. L. Foster, and F. Ardhuin, J. Geophys. Res. **113**, C09007 (2008).
[7] T. Hara, C. C. Mei, and K. T. Shum, Phys. Fluids A **4**, 1373 (1992).
[8] H. C. Earnshaw and C. A. Greated, Exp. Fluids **25**, 265 (1998).
[9] T. S. Jespersen, J. Q. Thomassen, A. Andersen, and T. Bohr, Eur. Phys. J. B **38**, 127 (2004).
[10] P. Nielsen, J. Geophys. Res. **86**, 6467 (1981).
[11] G. Vittori and P. Blondeaux, J. Fluids Mech. **218**, 19 (1990).
[12] J. Lebunetel-Levaslot, A. Jarno-Druaux, A. B. Ezersky, and F. Marin, Phys. Rev. E **82**, 032301 (2010).
[13] I. S. Aranson and L. S. Tsimring, Rev. Mod. Phys. **78**, 641 (2006).
[14] E. Foti and P. Blondeaux, Coastal Eng. **25**, 237 (1995).
[15] J. S. Doucette, Sedimentology **49**, 483 (2002).
[16] S. Balasubramanian, S. I. Voropayev, and H. J. S. Fernando, J. Turbulence **9**, 1 (2008).
[17] B. J. Landry, M. J. Hancock, and C. C. Mei, Coastal Eng. **54**, 694 (2007).
[18] A. B. Ezersky and F. Marin, Phys. Rev. E **78**, 022301 (2008).
[19] J. M. Pastor, D. Maza, I. Zuriguel, A. Garcimartin, and J. F. Boudet, Physica D **232**, 128 (2007).
[20] F. Marin, Coastal Eng. **50**, 139 (2004).
[21] D. H. Swart, *Delft Hydraulics Laboratory Report No. R968*. 1976.
[22] A. G. Davies, Coastal Eng. **4**, 23 (1980).
[23] F. Hering, C. Leue, D. Wierzimok, and B. Jähne, Exp. Fluids **23**, 472 (1997).
[24] F. Hering, C. Leue, D. Wierzimok, and B. Jähne, Exp. Fluids **24**, 10 (1998).
[25] S. S. Rogers, T. A. Waigh, X. Zhao, and J. R. Lu, Phys. Biol. **4**, 220 (2007).
[26] J. J. Van der Werf, V. Magar, J. Malarkey, K. Guizien, and T. O'Donoghue, Cont. Shelf Res. **28**, 1040 (2008).
[27] K. Gislason, J. Fredsoe, R. Deigaard, and B. M. Sumer, Coastal Eng. **56**, 341 (2009).
[28] M. S. Longuet-Higgins, Philos. Trans. R. Soc. London, Ser. A **245**, 535 (1953).